Heliyon 10 (2024) e24768

Contents lists available at ScienceDirect

Heliyon

journal homepage: www.cell.com/heliyon

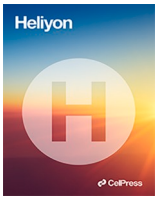

Research article

Simulation of the fluid dynamic and thermal behavior of an experimental passive cooling system of photovoltaic panels

Guido Abril-Macias [a,*], Juan Peralta-Jaramillo [a], Emerita Delgado-Plaza [a], Ian Sosa-Tinoco [a,b,1], Daniel Avilés [a,c]

[a] Centro de Desarrollo Tecnológico Sustentable, Escuela Superior Politécnica Del Litoral, Guayaquil, 090150, Ecuador
[b] Departamento de Ingeniería Eléctrica y Electrónica Instituto Tecnológico de Sonora, Mexico
[c] Facultad de Ingeniería Mecánica y Ciencias de la Producción (FIMCP), Escuela Superior Politécnica, Ecuador

ARTICLE INFO

Keywords:
Simulation
Fluid dynamics
Temperature
Transient
PVT
Cooling device

ABSTRACT

Solar energy capacity has increased significantly globally, with values above 800 GW produced by different systems. Among these, PVT panels can generate either electricity, heat, or both. As these systems present various issues associated with excessive temperature increases, cooling systems have been developed to control the temperature using fluids such as water. The article uses previous data from the Technologic Institute of Sonora, which analyzed various cooling device configurations and selected the best two options (B1 and B4) based on the panel efficiency. Using the boundary conditions and the predicted streamlines, a simulation was made in CFD programs, determining the correct parameters to replicate the system fluid dynamics. Several simulations were carried out using different turbulence models. After comparing the temperature contour diagram and the streamline, it was obtained that the k-ω turbulence model best describes the fluid's behavior. The transient analysis simulations allow us to determine that the B1 configuration delivers the best cooling effect as it presents the most homogeneous temperature profile. BIAS and RMSE were calculated to validate and contrast the results obtained experimentally, obtaining values of 0.8675 and 1.8981, respectively.

1. Introduction

1.1. PVT systems

In the realm of renewable energy, solar power stands out as a prominent player, exhibiting a remarkable growth trajectory in recent years, with an increase of over 800 GW in installed capacity. This expansion has been particularly notable in regions such as China and the European Union, where the solar energy capacity witnessed significant increments of more than 200 GW and 100 GW, respectively, in 2020 [1,2].

It is noteworthy to acknowledge that photovoltaic (PV) installations can be classified into three distinct categories: grid-connected

* Corresponding author.
E-mail addresses: gabril@espol.edu.ec (G. Abril-Macias), jperal@espol.edu.ec (J. Peralta-Jaramillo), eadelgad@espol.edu.ec (E. Delgado-Plaza), ian.sosa@itson.edu.mx (I. Sosa-Tinoco), deaviles@espol.edu.ec (D. Avilés).

[1] We would like to thank ITSON's Programa de Fomento y Apoyo a Proyectos de Investigación (PROFAPI-2023-050) for funding provided for this study.

https://doi.org/10.1016/j.heliyon.2024.e24768
Received 4 August 2023; Received in revised form 29 December 2023; Accepted 14 January 2024
Available online 22 January 2024

Nomenclature

Symbols

M	Meter
mm	Millimeter
°	Tilt angle
Kg	Kilogram
N	Newton
KN	Kilo newton
l	Liter
W	Watts
kW	Kilowatts
K	Kelvin Degree
°C	Celsius Degree
H	Hour
Q	Flow
d	Diameter
m/s	meter/second
W/mˆ2	Watts/square meters
atm	Pressure atmosphere

Abbreviations

ESPOL	Escuela Superior Politécnica del Litoral
PVT	Photovoltaic - Thermal
PV	Photovoltaic
ITSON	Instituto Tecnológico de Sonora
SOC	Standard Operation Conditions
RMSE	Root Mean Square Error
SST	Shear Stress Transition
PCM	Phase Change Materials
TE	Thermal/electric
RANS	Reynolds Average Navier-Stokes

systems, isolated systems, and hybrid systems. Grid-connected systems employ inverters to transform the direct current (DC) generated by the PV system into alternating current (AC), which seamlessly integrates into the conventional power grid. In contrast, isolated systems are commonly deployed in remote or secluded areas [3]. These systems harness solar radiation to provide power for various household appliances, and their unique advantage lies in the ability to store surplus energy in batteries for use during periods of limited solar radiation, ensuring uninterrupted electricity generation.

Furthermore, there exist hybrid systems that combine multiple energy sources, such as solar panels and gasoline generators. These systems distinguish themselves from grid-connected ones as they primarily rely on solar energy as the primary energy source rather than as a supplementary power source [4].

1.2. PVT system issues

A category of solar energy collection systems that combines photovoltaic and thermal technologies is known as photovoltaic thermal systems or PVT. These systems are advantageous as they optimize solar energy utilization for both electricity generation and heat production [5]. Nonetheless, challenges can arise due to factors such as environmental conditions, site placement, and neighboring infrastructure, despite these benefits.

Tables 1 and 2 present the most common problems during the useful life of a thermal photovoltaic panel that causes loss of efficiency in these panels. An example is the temperature increase in photovoltaic panels, which is counterproductive for the generation of electricity and its subsequent use [6].

Table 2 highlights a range of issues affecting photovoltaic solar panels, with a specific focus on hot spots. These hot spots arise from localized temperature concentrations within the panel cells, leading to overheating peaks. The consequences of these peaks can be severe, with the potential to inflict permanent damage on the device. This damage can manifest in two detrimental ways: firstly, by diminishing the system's efficiency, resulting in a reduced power generation capability, as noted in Ref. [13]. Secondly, it may render the entire module useless, irrespective of its cell configuration or type, as indicated in Refs. [14,15]. The overarching impact of these hot spots is a significant reduction in the power generation efficiency of photovoltaic solar panels.

To mitigate or entirely circumvent this adverse effect, it is imperative to implement an optimal cooling system. Such a system is essential to minimize or eradicate the detrimental consequences of hot spots on photovoltaic panels.

Table 1
Causes of loss of efficiency.

Author	Date	Ref.	Cause
L. Piotrowski	2020	[7]	Different weather conditions Exposure to the environment
A. Kandeal	2020	[8]	Climate, wiring, shade, circuits, connections
M. Mattei	2006	[9]	Wind Speed
N. Aste	2016	[10]	Material Quality Shadow Temperature Peaks Irradiation Behavior Connections Convection - Conduction
M. Fuentes	2017	[11]	Efficiency losses and temperature rise
M. Mohanraj	2019	[12]	Temperature
M. Suzuki	2021	[13]	Temperature

As can be seen in Table 1, the reduction in efficiency is a recurring situation in photovoltaic systems derived from the increase in temperature.

Table 2
Problems present in PVT systems.

Author	Date	Ref.	Problem
L. Piotrowski	2020	[7]	Degradation due to lack of cooling
M. Mattei	2006	[9]	Reduction of electrical efficiency due to temperature increase
N. Aste	2016	[10]	Thermal losses
M. Fuentes	2017	[11]	Temperature Rise Energy losses Poor thermal contact
M. Suzuki	2021	[13]	Efficiency losses and temperature rise
K. Kim	2013	[14,15]	Hot Spots
A. Pandian	2016	[16]	Hot Spots

Photovoltaic panels operating without adequate cooling can experience a considerable decline in efficiency, potentially reaching only 8–9% of their nominal power generation capacity. However, with the integration of a suitable cooling system, the efficiency can be elevated to a range of 12–14 %, as outlined in Ref. [16]. This enhancement is contingent on the effective management of uniform cooling, as highlighted in Ref. [17]. Neglecting this aspect may result in an escalation of temperature, exacerbating the hot spot issue.

In response to these challenges, numerous studies have been conducted to enhance the performance of photovoltaic panels and mitigate hot spot effects. These efforts include modifications to the panel's infrastructure, such as introducing an air gap to prevent overheating, as discussed in Ref. [18]. For multiple module systems, it is advisable to maintain a gap within the range of 0.12–0.15 m, while for single module systems, a gap of 0.14–0.16 m is recommended, as suggested in Ref. [19].

Furthermore, other strategies have been explored, including the utilization of phase change materials (PCMs) through the integration of PCM modules, as detailed in Refs. [20,21]. Additionally, forced air circulation cooling systems employing fans and air channels or utilizing dew pulses have been considered, as potential solutions to manage panel temperature and hot spot issues. Moreover, Schottky bypass diodes, as discussed in Ref. [23], are primarily employed in scenarios involving shading on the panel, where obstacles obstruct sunlight from reaching the photovoltaic cells, leading to reduced energy production. In cases with substantial shading, bypass diodes redirect the current flow to prevent congestion in shaded areas, effectively addressing this problem.

Thanks to technological advances, new designs of photovoltaic systems have been developed with different results in terms of reducing energy losses [24,25] demonstrating that it is possible to reduce the effect of hot spots by up to 17 %.in most systems [26].

Finally, software that works with computational fluid dynamics or CFD is being used [27], which allows both 3D modeling and behavior simulation for gases and liquids used as heat transfer fluids in cooling systems.

This document seeks to contribute to the process of validation of technological solutions developed to reduce the effects associated with the increase in temperature and the presence of hot spots in the PV modules. For the case presented, the Technological Institute of Sonora [13] proposes a cooling system using brine as heat transfer fluid because seawater is used for the reverse osmosis desalination process. Allowing the use of various configurations for workflow management and optimization of the cooling effect in photovoltaic panels.

Therefore, the general objective of this document is to evaluate two flow distribution configurations of an experimental cooling system for photovoltaic panels in a process before desalination. For this, simulations will be conducted using computational fluid dynamics, which will analyze the behavior of the fluid in both configurations, as well as the heat transfer to the device and fluid. Finally, the results of the simulation will be validated qualitatively with previous experimental results conducted by Suzuki et al. [13].

2. Theoretical framework

2.1. Solar energy

One of the main sources of energy used during several decades as a renewable resource is the sun. Among the technologies developed for the use of this natural source are solar concentrators, panels, and photovoltaic thermal hybrids or PVT. The figure shows a comparative scheme between systems (Fig. 1).

PVT stands out among the solar harvesting systems since it can be used to generate both electrical and thermal energy and has a wide range of applications such as drying, water heating, and electrical sources, among others (see Fig. 1). These systems consist of the following parts (Fig. 2).

2.2. Recent advancements in solar system research

In addition to the advancements in solar technology mentioned earlier, several research studies have explored the performance and efficiency of solar systems in Iraq. These investigations encompass both flat plate solar systems and hybrid photovoltaic thermal (PVT) systems, shedding light on their adaptability to changing parameters and regional climate conditions. One study analyzed flat plate solar systems in Duhok City, Iraq, in May 2019, examining their energetic and exergetic efficiencies and the influence of climatic conditions on performance. Another study focused on PVT systems in Dohok City, Northern Iraq, highlighting the potential for achieving both thermal and electrical efficiencies and recommending the active mode utilization of PVT water systems for sustainable energy generation. Further research in Zakho City, Iraq, emphasized the advantages of PV solar systems with tracking technology, which significantly improved electrical output power, reduced energy costs, and cut annual CO2 emissions. Lastly, an analysis of a grid-connected PV solar system at the University of Zakho revealed its efficiency, low cost of energy, and capacity factor, making it a

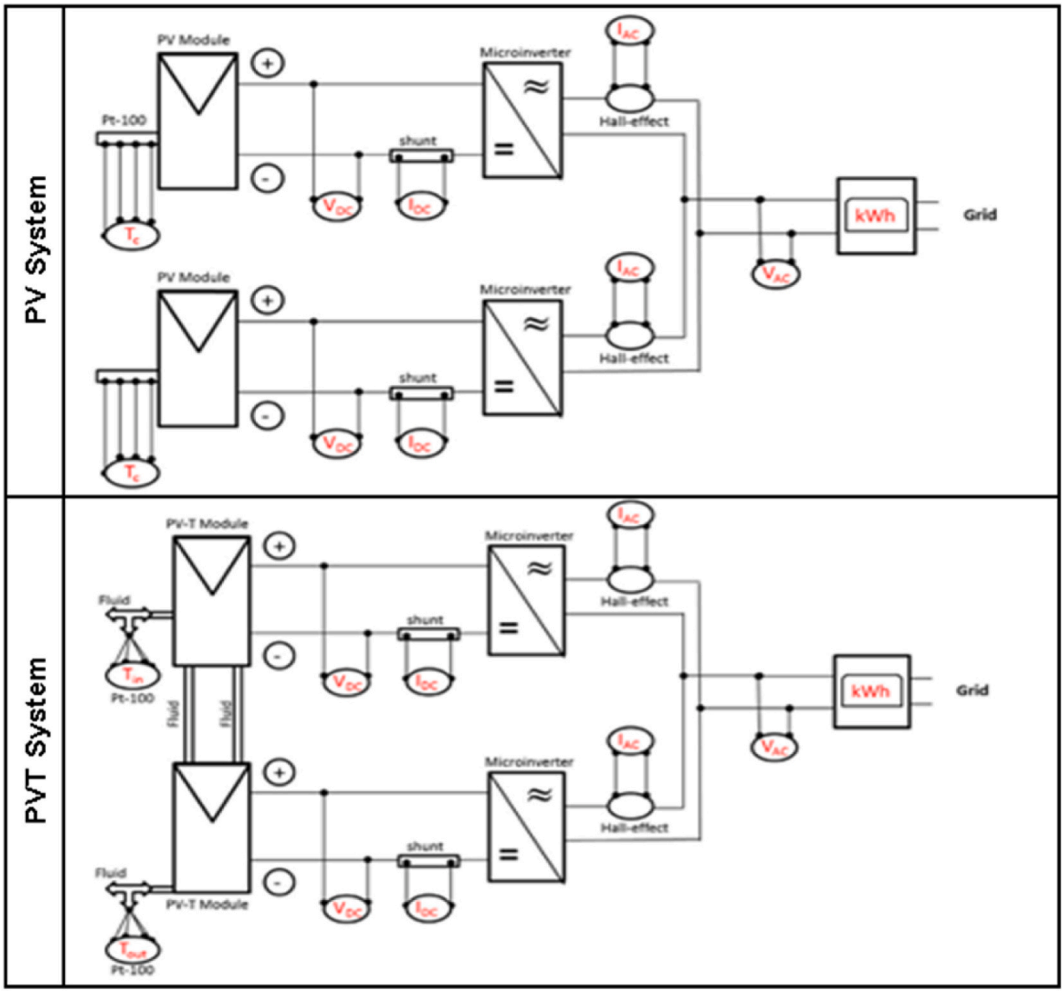

Fig. 1. Comparative schemes of solar thermal and photovoltaic systems.

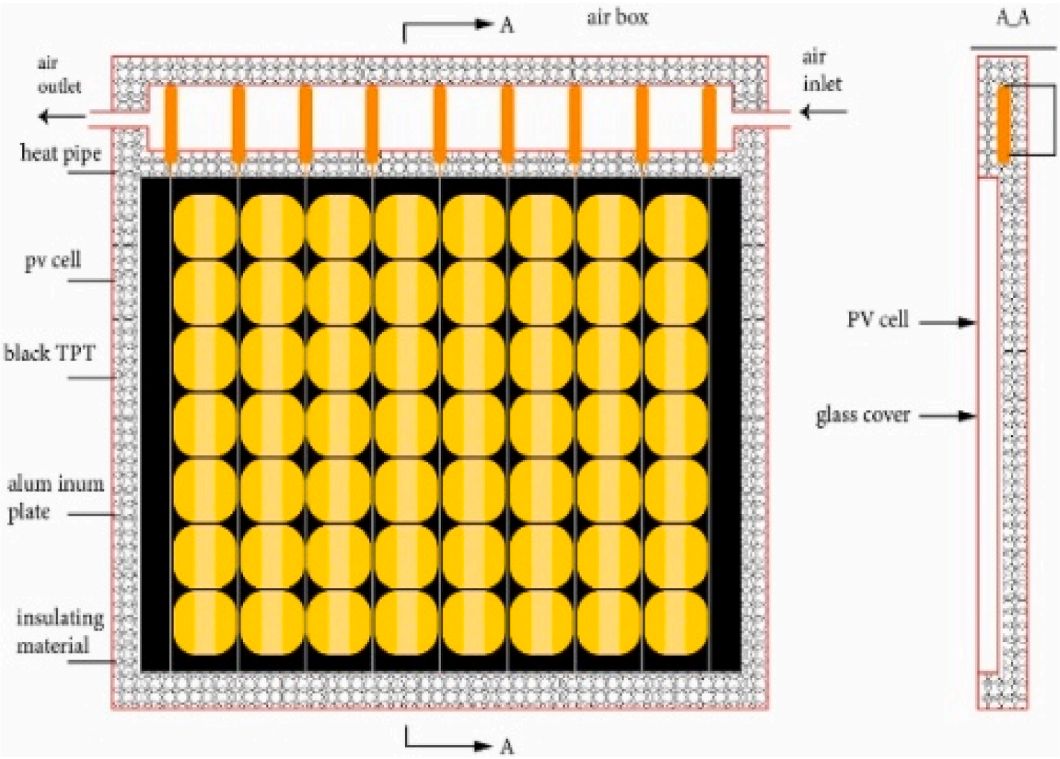

Fig. 2. Components of a photovoltaic panel [28].

reliable source of electricity. These studies provide valuable insights for potential investors in PV technology ventures in Iraq, emphasizing the practicality and performance of solar energy systems in the region [29–32].

2.2.1. *Cooling technologies*

Because PVT systems make use of solar radiation, they tend to raise their temperatures above the optimal operating range. This can cause significant efficiency losses, as well as the phenomenon called Hot Spots. To avoid these drawbacks, over the years different cooling technologies have been developed to be implemented in PVT systems. These technologies can be separated into two groups.

2.2.1.1. Conventional cooling technologies with liquid (water) or gaseous (steam) fluid. In the first case, the heat transfer fluid is a liquid, for example, a refrigerant R32, water, or brine. These systems have elements such as pump, water tank, valves, and flowmeter, among others. (Fig. 3). For the case study, the latter is used. because it seeks to take advantage of the heat received from the sun to conduct a pre-treatment of seawater that will go through a process of desalination by reverse osmosis.

The second case is refrigeration technologies that use a gas as a heat transfer fluid, for example, water vapor. They can be separated into systems by natural or forced convection depending, for example, on the use of fans or blowers. In general, they tend to be systems similar to a hybrid between a PV panel and a heat exchanger, liquid immersion, or microchannels [33].

2.2.1.2. New cooling technologies. This technology group comprises the most recently developed cooling systems, such as the phase change materials or PCM mentioned above. The results of several investigations carried out previously [20,34] conclude that the use of PCM can suppress the thermal effects of solar radiation in a thermoelectric system (TE) composed of PV and PCM panels also called the PV-PCM-TE system [22]. Furthermore, when used in a hybrid system together with cooling employing water, it can generate significant cooling effects depending on the angle of the wind current [34]. It is also worth mentioning the use of nanofluids which have been shown to have greater efficiency than conventional systems that use water [35]. Finally, one of the most recent technologies can be added, this being an Emulsion Filter [36] which takes advantage of ultraviolet radiation, the light wave from the environment close to the experiment, and even infrared radiation.

2.3. *Simulation and influence factors*

Currently, due to the complexity of these systems, study methods have been implemented through simulations (operational, experimental) These simulations are procedures in which a scheme of the system to be studied is used and conditions and mathematical models are applied according to the physics that governs it. For the analysis, it is necessary to review several factors that directly

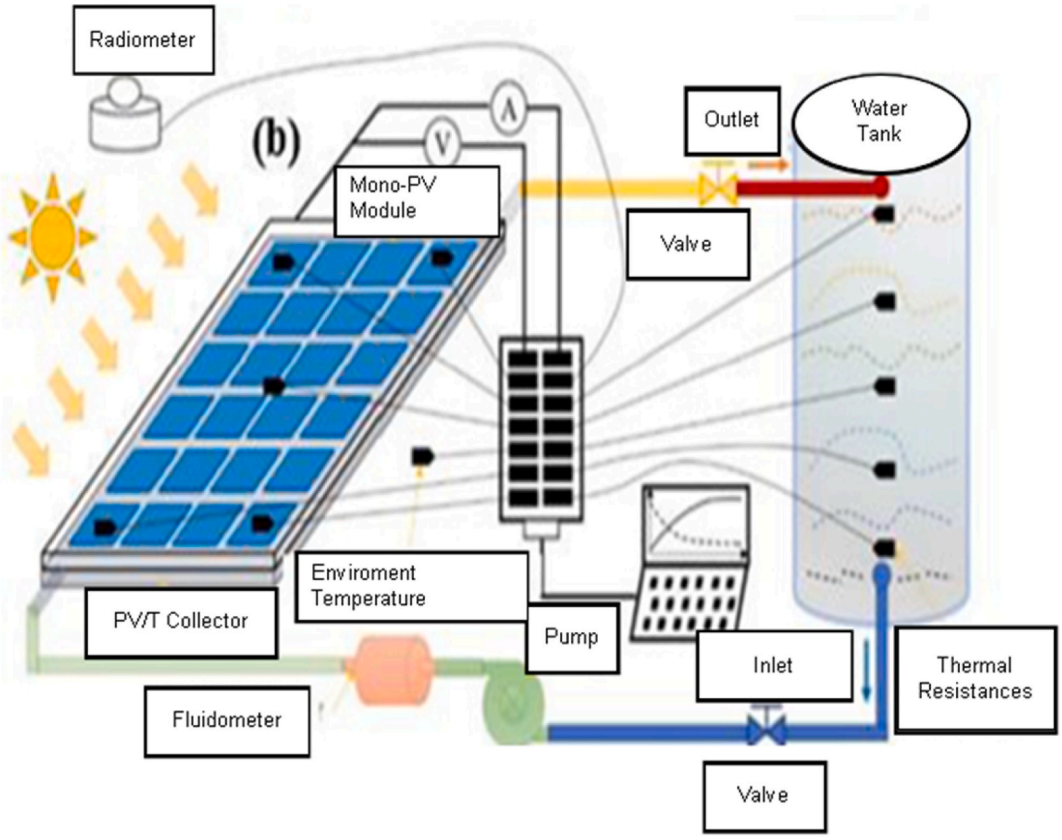

Fig. 3. Scheme of the cooling system using liquids.

influence the procedure, which we divided into three groups of variables [9,27].

2.3.1. Climatology

Climatic factors depend on the environment in which the study or experiment is conducted. These factors vary by geographic location and, although they cannot be controlled, they directly affect various experimental results. Some examples like temperature and wind speed are shown in Table 3.

As can be seen in the table mentioned above, Solar Irradiation is 1 kW per area unit, and the ambient temperature ranges between 25 and 30 °C depending on the geographic location of the system. The area of the implementation of the experimental prototype presents significant variations in wind speed and solar irradiation; these fluctuations must be considered when performing simulations of behavior in the transient regime.

2.3.2. Geometric model

Geometric models are the representation of the physical shape or geometry of the system to be simulated. It is of foremost importance to remember that the measurements and dimensions must be as exact as possible since any failure in this section can cause

Table 3
Relevant environmental factors in cooling simulations.

Author	Date	Reference	Environmental Temperature. (K)	*Solar R.* $\left[\frac{W}{m^2}\right]$	*Wind Speed* $\left[\frac{m}{s}\right]$
C. M. Jubayer	2016	[27]	303	–	1, 5 & 10
M. Mohanraj	2019	[12]	305	550	2.5
A. Almuwailhi	2021	[37]	298	–	N/A
M. R. Zargarabadi	2020	[38]	298	985	1–1.4
Fabrizio Leonforte	2016	[10]	298	–	–
Levent Bilir	2021	[39]	298	–	1, 5, 7, 10
M. Eslami	2021	[40]	300	600	4
L. J. Piotrowski	2020	[7]	298	–	–
Jun Yang	2018	[41]	298	667.2	0

an exponential growth of error in the results [42].

In Table 4, some geometries used for the study of cooling systems in photovoltaic solar panels are shown, as well as the type of fluid heat transfer used as a coolant. It can be seen that the isometric bodies are the most used geometry when running the simulations, although there are also cases in which simpler geometries are used where an inclined plane was used to represent the photovoltaic panels [41] or cases in which a section was used to represent the mesh [40].

Regarding the mesh geometry, in Table 4 it can be seen that most of the authors opted for a standard geometry, that is, tetrahedral, whether they are rectangles or squares. In other cases, it is not mentioned the shape of the meshing, but this is due to the method of the experiment finally we have the cases of those who used a triangular geometry to capture the profile of more complex figures and increase the precision, as well as the authors who have used a hybrid geometry, that is, a mixture of the standard and the triangular more accurately.

It is important to note that a single fluid is not always employed, having occasions when both air and water are employed [12]. Furthermore, the table shows that both fluids are used equally for this cooling process, being that of the nine examples, four use water and four use air, the remaining example being the hybrid case.

2.3.3. Standard operating conditions

Finally, the third group is the standard operating conditions or SOC. This refers to the restrictions, physical or operational, that each experiment has, either in terms of fluid flow or the desired inlet or outlet temperature, among other configuration changes. Table 5 shows some examples of these conditions.

As can be seen, each experiment has several different constraints. Especially the angle of inclination and the environmental conditions since these differ according to the location of the experiment. In certain cases, there may be similarities where the panels have 36 cells [27,40], but in general, each case has its restrictions.

2.4. Fluid behavior simulation

Due to the complexity of capturing the behavior of the fluid within the systems previously commented, a widely used alternative is to perform a computational simulation. This dynamic is a great support for researchers by being able to predict failures, accidents, and unfavorable situations in general while at the same time providing valuable information to improve the system in such a way that the previously mentioned problems are avoided. The simulation process consists of five steps, which are.

3. Geometry Definition
4. Meshing
5. Definition of Parameters and Operating Conditions
6. Iterative process

3. Results processing

In each of these steps, several factors are considered, for example, in the definition of geometry the measurements of the system's component to be evaluated and the material of which the geometric model is composed. In meshing, geometry-dependent criteria are used to select the most appropriate mesh to solve the problem. In the stage of definition of parameters and conditions of operation the properties of the fluid, the solid within which it flows, and the initial and boundary conditions are established. Also, in this section, the turbulence model that best represents the phenomenon of the behavior of the fluid is selected. In the iterative process, the residuals are established, which are the error ranges allowed for the parameters obtained from the turbulence model, as well as the number of iterations that the program will conduct until reaching a desired convergence. Finally, in the results processing, graphs of various fluid properties can be obtained such as pressure, temperature, speed, and drag force, among others.

3.1. Computer simulation of the prototype

Knowing the advantage that computer simulation gives, it must be considered that the choice of the program to use can also affect

Table 4
Experimental Meshing geometries.

Author	Date	Reference	Body Geometry	Mesh Geometry	Fluid Type
Chowdhury M. Jubayer	2016	[27]	XZ Plane Tilt 25°	Standard - Hexahedral	Air
M.Mohanraj	2019	[12]	Isometric	Standard	Mix
A. Almuwailhi	2021	[37]	Isometric	Standard	Water
Dirk Goossens	2018	[43]	Isometric	Triangular	Air
Mehran Rajabi Zargarabadi	2020	[38]	Isometric	N/A	Water
Fabrizio Leonforte	2016	[10]	Isometric	N/A	Water
Levent Bilir	2021	[39]	Isometric	Standard – Hybrid	Air
M. Eslami	2021	[40]	Section	Triangular	Air
Jun Yang	2018	[41]	Isometric	N/A	Water

Table 5
Conditions of Operation quoted.

Autor	Restrictions
Chowdhury M. Jubayer [27]	Three wind speeds (1, 5, 10 m/s). 10 m high. Latitudes between 30° and 45°. Inlet temperature 30 °C. Flow in “Atmospheric equilibrium"
M.Mohanraj [12]	Tilt angle = 11°. Tank of 500 l. 380 W pump. 4 PV panels. PV panel generation range [400–1000] W. Ten-minute data. Water velocity 1 m/s
A. Almuwailhi [37]	The angle of inclination = 23° fixed. Relative humidity and dry bulb = Riyadh climate in summer. Two panels with 72 cells (36 each). Forced convection with fan
Mehran Rajabi Zargarabadi [38]	30° cooling nozzles of the PV Panel. Ten-minute data from 11:30 to 15:30. 36 cells
Fabrizio Leonforte [10]	Isotropic system absorption Mass flow = 0.055 kg/s. Tank capacity = 200 l. 25° tilt Coefficient of heat loss = 5 W/m2K Required power = 1.5 W Inlet and outlet temperature range = [10 °C–90 °C].
Levent Bilir [39]	30° tilt. Convection throughout the system except on the top side. Cooling channel material = Aluminum. Outlet pressure = Atmospheric. 60 cells (2 groups of 30)
M. Eslami [40]	36 cells. RANS. Tilt 20°. No slip Uniform wind speed 4 m/s (inlet) pressure (outlet).
Dirk Goosens [43]	Maximum wind speed = 5 m/s 3.5 or 5.5 cm openings for air intake

its performance since not all of them contain the same number of processes or can simulate the same situations. For the case study, the use of two programs has been chosen since it will seek to evaluate the behavior of the fluid in a transient and stable state. Therefore, the ANSYS Fluent program will be used to study the behavior in a steady state, and the Solid Works program for the transient state.

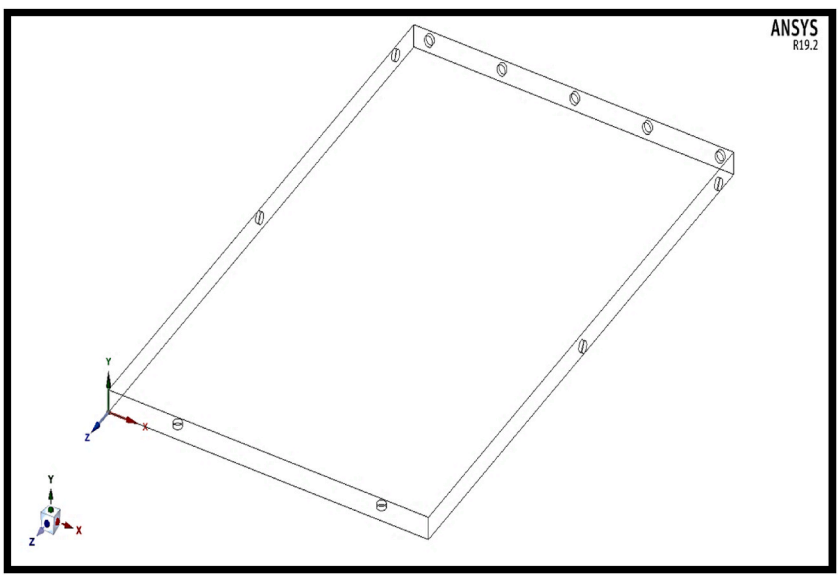

Fig. 4. Geometry of the device. Wireframe view.

4. Methodology

4.1. Fluid behavior

4.1.1. 3D design – geometry

The methodology consists of the design or geometry model, mesh selection, constraint settings, and the selection of turbulence model for stationary state analysis in ANSYS. For the transient analysis done in SolidWorks, a similar procedure was followed, first defining the geometries to be analyzed, performing a cubic mesh, defining initial and boundary conditions, and adding the flow simulation tool where the study variables were added.

The device to be simulated resembles a “box" with dimensions of 992 mm × 1640 mm which has perforations with a diameter of one inch, which can be defined as inputs and outputs (Fig. 4).

For this experiment two models will be used when using two configurations of the device (Fig. 5 & Fig. 6). These models were selected for owning the best results according to studies previously conducted at ITSON [13]. The model’s solid was taken to be glass.

4.1.2. Mesh selection

Continuing with the procedure, a standard mesh was performed (Fig. 7), automatically generated to the geometry and then guided by the concept of quality, observing the values of orthogonality (tendency to 1) [44] and skewness (tendency to 0) [45]. Apart from this, a refinement was made using the “sizing" option and selecting four edges in the extremes, and then instead of using the element size, editing the number of divisions. Besides, an attempt was made to leave a greater density of elements in the key areas, in this case, fluid inlet and outlet sections [46]. Other mesh configurations can be seen in Table 6 and its result can be seen in Fig. 8.

4.1.3. Initial and boundary conditions

The initial conditions used were the following.

9. Initial flow: 1 l/min & 2 l/min
10. Initial temperature: 25 °C
11. Atmospheric pressure: 1 atm
12. Number of entries:7

Since we have 7 inlets, the initial flow that passes through each of these is shown in the equation below (Equation (1)).

$$Q_{in} = \frac{Q_i}{n_{in}} = \frac{1}{7} = 0.142857 \left[\frac{l}{min}\right] \quad \text{Equation 1}$$

with the initial flow, it is possible to determine the inlet velocity of the experiment using the following conversion formula (Equation (2)).

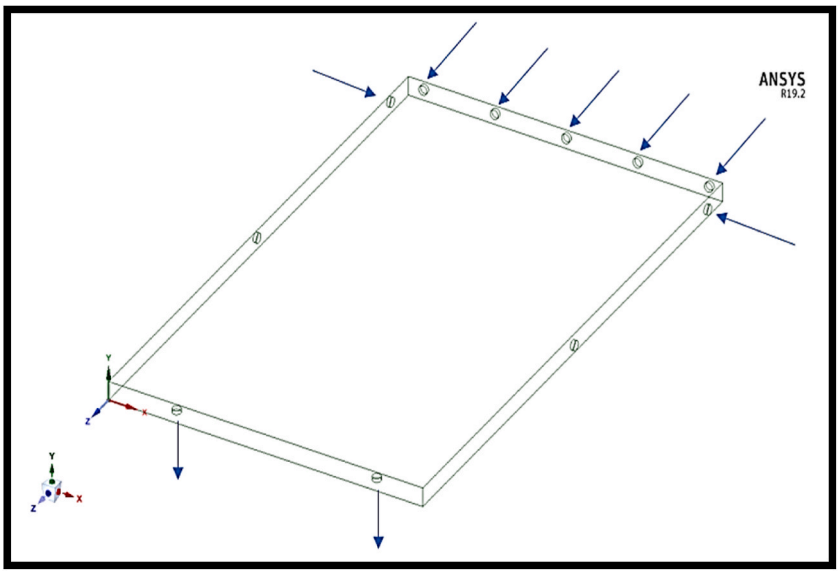

Fig. 5. B4 Configuration.

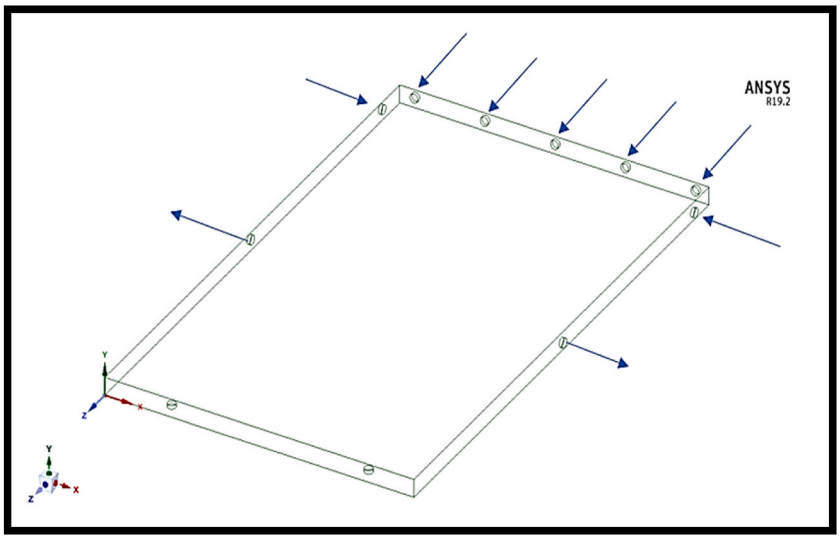

Fig. 6. B1Configuration.

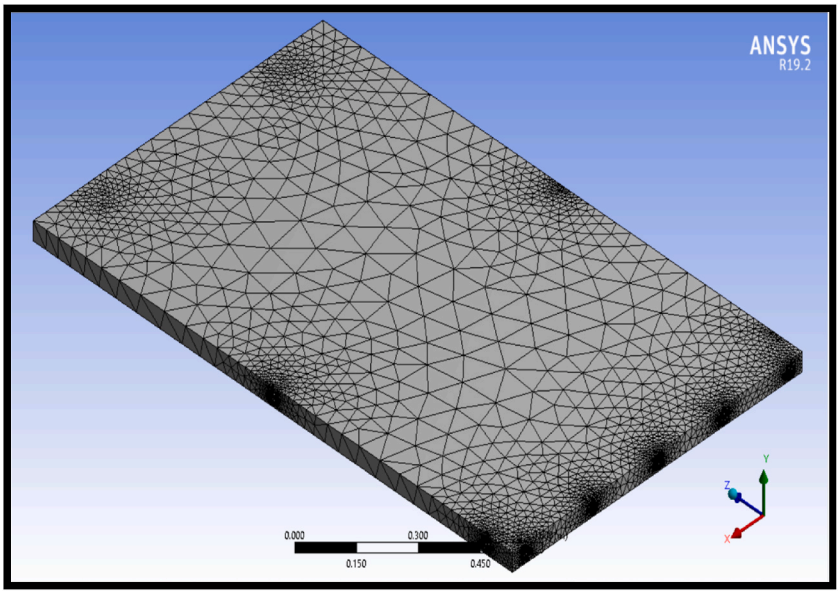

Fig. 7. Standard meshing.

Table 6
Mesh set up.

Orthogonality	Trend to 1
Skewness	Trend to 0
Sizing # de Divisions	$n = \frac{l_{máx}}{2} = \frac{1640}{2}\ [mm]$ $n = 820$
Behavior	Rough
Bias	- - — - -
Bias Factor	1.5

$$V_{T_{in}} = Q_{in}\left[\frac{l}{min}\right] x \left(\frac{1\ min}{60 seg}\right) x \left(\frac{0.001 m^3}{1 l}\right) x \left(\frac{4}{\pi d^2}\right)\left[\frac{1}{m^2}\right];\ V_{T_{in}} = 0.0047\frac{m}{s} \quad \text{Equation 2}$$

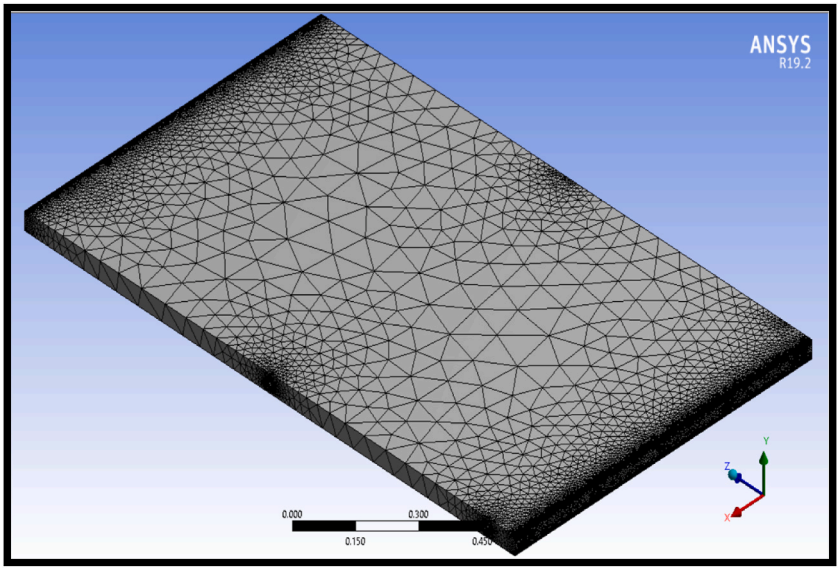

Fig. 8. Discretized meshing.

Where.

$V_{T_{in}}$ = Input speed
Q_{in} = Initial flow
d = Diameter of inlets and outlets = 1 in or 0.0254 m

4.1.4. Turbulence model

According to the reviewed literature [42,43,47–49] the k-ε, k-ω, and SST models were selected, so each of these was tested to determine their influence on the simulation of fluid behavior.

A parameter considered to select the best possible model is the Reynolds Number, which is obtained using the next equation (Equation (3)):

$$Re = \frac{\rho VD}{\mu} = \frac{V_{T_{in}} d}{v} = \frac{0.0047 * 0.0254}{8.9x10^{-7}} = 134.134 \quad \text{Equation 3}$$

where:

$V_{T_{in}}$ = Input speed

v = Water's kinematic viscosity at 25 °C $\left(8.9x10^{-7}\frac{m^2}{s}\right)$.

It should be noted that this software works with the infinite element method by applying the following governing equations for the simulation of the fluid's behavior (Equations (4) and (5)) and heat exchange (Equation (6)) respectively:

$$\frac{d\rho}{dt} + \nabla \bullet \rho \overrightarrow{v} = 0 \quad \text{Equation 4}$$

$$\frac{\partial(\rho u_i)}{\partial t} + \frac{\partial(\rho u_i u_j)}{\partial x_j} = \mu \frac{\partial^2 u_i}{\partial x_j{}^2} - \frac{\partial P}{\partial x_i} + \rho g_i \quad \text{Equation 5}$$

$$\frac{\partial(\rho_i)}{\partial t} + div(\rho_i \boldsymbol{u}) = -pdiv\,\boldsymbol{u} + div(\kappa\, grad\, T) + \Phi + S_i \quad \text{Equation 6}$$

4.1.5. Comparison

The generation of a contour that represents the temperature profile was employed to be able to determine the heat spots that are generated by the movement of the fluid.

4.2. Heat exchange

For this analysis, a CFD program different from the previous one was used due to the complexity of analyzing transient, but similar steps were followed. Due to this several values used and found in the previous simulation were used as input values or conditions to

obtain better results.

4.2.1. Geometry

Two geometric models were designed for this CFD software, using the previous simulation model as a reference, one for each configuration. The geometries corresponding to configurations B1 and B4 are shown below (Fig. 9).

4.2.2. Initial conditions

The same conditions were used for the calculation of the streamlines.

Additionally, data tables concerning time were used to define the behavior of environmental temperature and irradiation. These tables were obtained from experimental data conducted by the Technological Institute of Sonora, Mexico [13].

4.2.3. Influencing factors

The same information was used as in the previous case, adding the data table on the variation of temperature and radiation as a function of time per hour, obtained during the experimental process for the date July 24, 2018, from 6:00 a.m. to 5:00 p.m. when the ambient temperature and actual radiation were known.

4.2.4. Comparison

Thermal images obtained from a previous experimental process [13] were used to do a qualitative comparison of the temperature profiles obtained in both CFDs, both in steady and transient states. In this way, we tried to find similarities in the areas of the graph where there is a temperature variation, and that said variation is within the same range both experimentally and in the case of the simulation (Figs. 10 and 11).

5. Results analysis

In the study case, to establish a more detailed behavior of the fluid, the configurations were analyzed both in stationary and transient states.

5.1. Fluid behavior

In the first place, the simulations of the different configurations in steady state were conducted, and the contour curves and a graphic qualitative comparison with the thermography of the pilot testing stage were done [13].

Tables 7 and 8 show the graphs of the fluid behavior and the temperature contour for the B4 and B1 configurations respectively and the four simulated turbulence models.

Performing a qualitative comparison, we can see that the change in the turbulence model affects the resulting temperature contour lines the most, with the SST and Reynolds stress models showing the most variations in the temperature contour graphs.

On the other hand, no significant changes are visualized about the streamlines, except in limit zones or panel walls derived from the vicinity of the outlets.

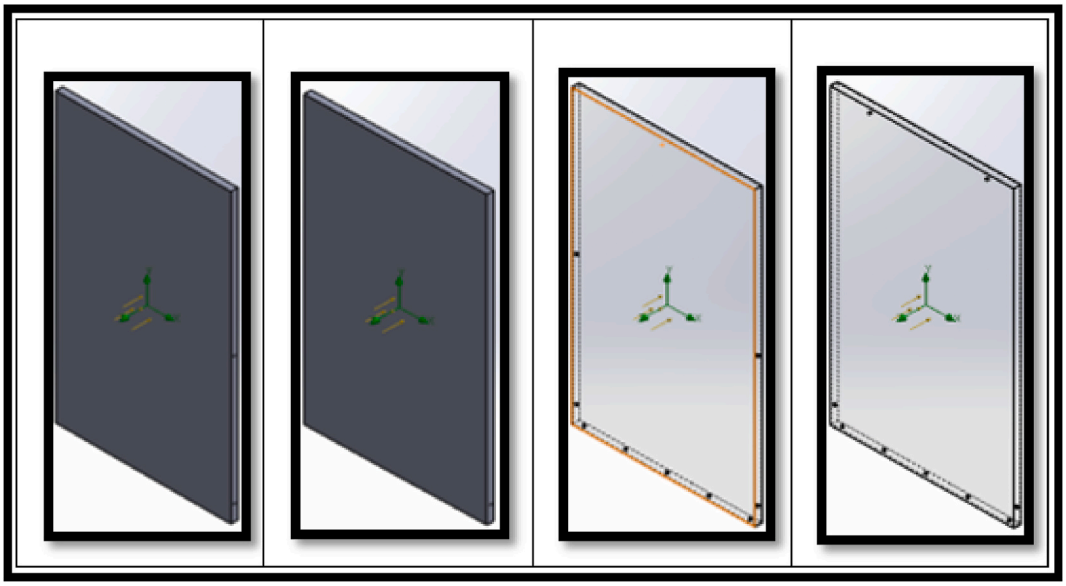

Fig. 9. From left to right: Configurations B1 and B4 in solid view and wireframe view.

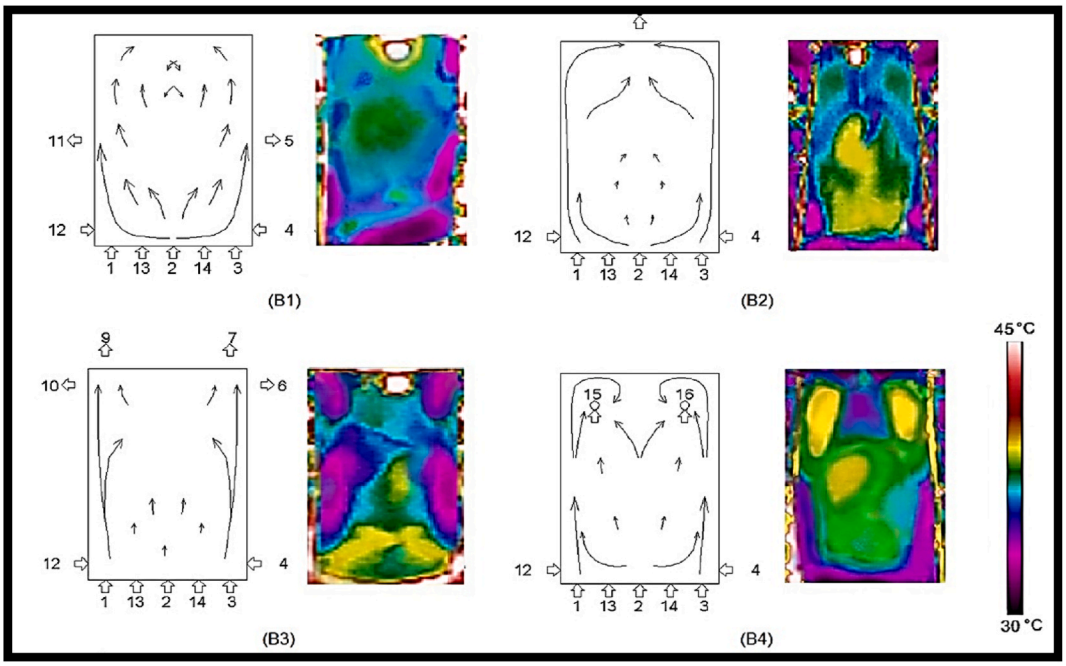

Fig. 10. Thermography and tentative diagram of the fluid behavior of configurations B1, B2, B3 and B4 [13].

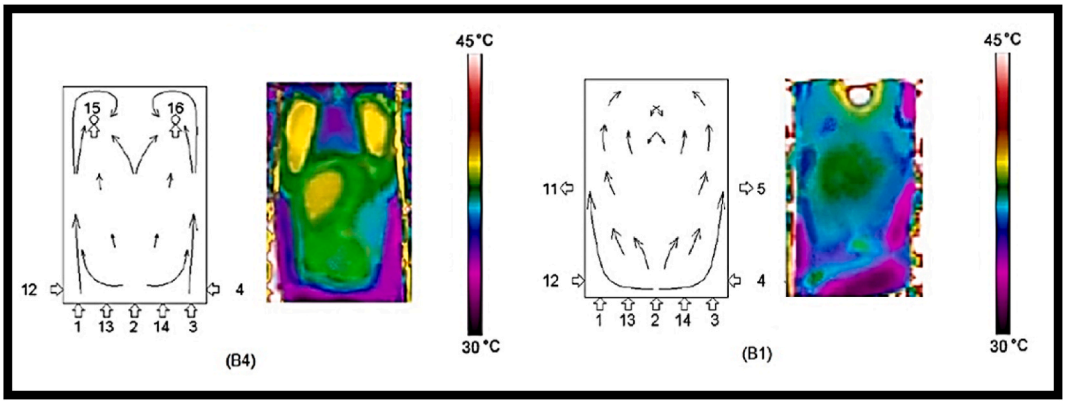

Fig. 11. Thermography and fluid behavior for configurations B1 and B4 [13].

In practice, for the simulation of the temperature isolines, external elements that can cause points or zones of additional color in the configurations are not considered, such as the electric motor.

In addition to Tables 7 and 8, we can use Table 9 to make a better comparison of the route shown by the streamlines in the simulation in contrast to the established graphs.

In this table, it can be seen that the prediction of the behavior of the fluid had a greater precision for the case of the B4 configuration, with only certain inconsistencies in the lower area, while in the case of B1 the contrast that exists between both trajectories, especially in the upper and central area where certain intersections are located in the experimental behavior which do not appear in the simulation carried out.

5.1.1. Heat exchange–stationary

With the data obtained, the temperature comparison can be seen in Table 10. In the case of configuration B1 there are certain appreciable similarities, but the same cannot be said of configuration B4. Another point to analyze is the variability of the temperature shown in each configuration since the B1 has less variety of colors than the B4.

However, it can be seen that in neither of the two cases is there a significant similarity between the outlines of simulation and experimental thermography.

At this point, it should be emphasized that there are several limitations to performing a stationary analysis such as [47,48].

Table 7
Stationary results of Streamlines and Temperature. B4 Configuration.

Turbulence Model	Streamlines	Temperature
$k-\varepsilon$	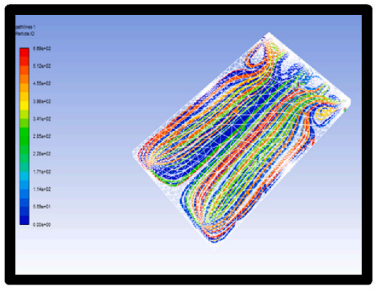	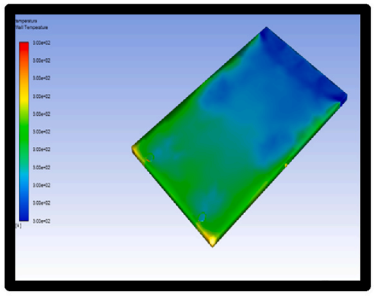
$k-\omega$	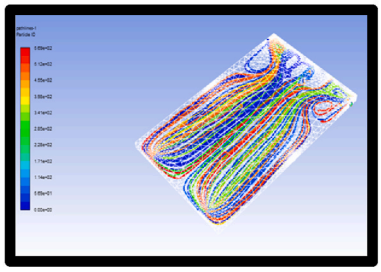	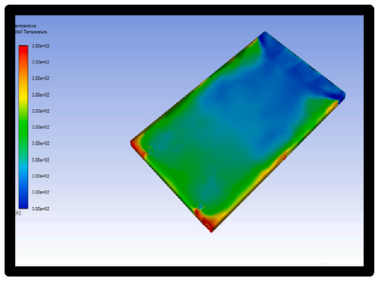
SST	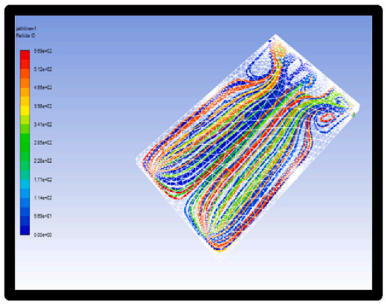	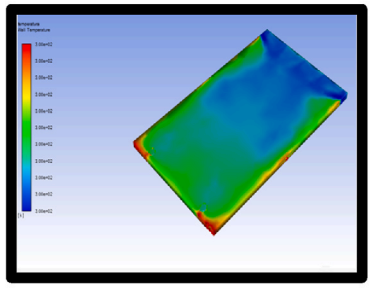

14. Results Overestimation
15. Conditions Idealization
16. Omission of external variables fluctuation
17. Less experimental control by intervening with fewer variables.

Therefore, to set the optimal configuration, the two best configurations will be analyzed with a transient state.

5.2. *Thermal exchange – transient*

When using the tool for the simulation of the transient state, graphs of isolines of the fluid temperature were obtained. Figs. 12 and 13 show the temperature profile in a three-dimensional section of the model, while Table 11 shows the temperature comparison of configurations B1 and B4 respectively in the transient state.

Continuing with the analysis, Table 12 shows the comparison of the data obtained from the simulation in transient with the information acquired experimentally. For this, information from 4 days of experimentation corresponding to August of the year 2019, was obtained from the Meteorologic Lab at ITSON, during which different time steps were taken.

The values from this table, have been adjusted (Fig. 14) to determine the relationship between these parameters.

As can be seen in Fig. 14, there is a correlation between the values of ambient temperature and the difference between experimental and simulated temperatures. This correlation corresponds to the following equation (Equation (7)).

$$\Delta T = 0.489 T_{env} - 17.823; \Delta T = T_{exp} - T_{sim} \quad \text{Equation 7}$$

Table 8
Stationary results of Streamlines and Temperature. B1Configuration.

Turbulence Model	Streamlines	Temperature
$k-\varepsilon$	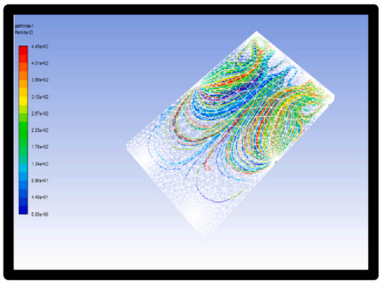	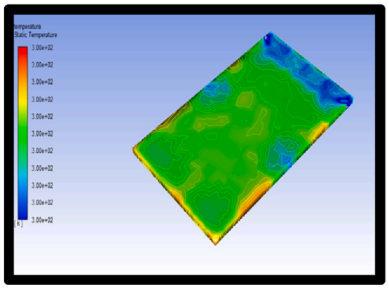
$k-\omega$	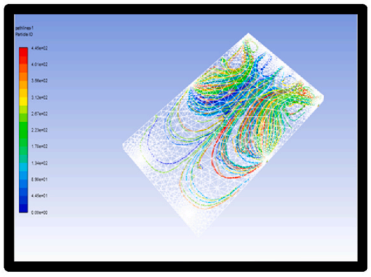	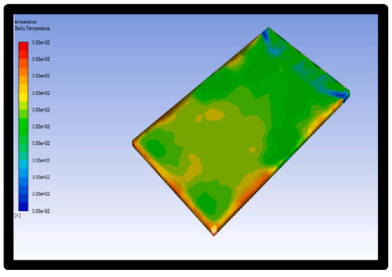
SST	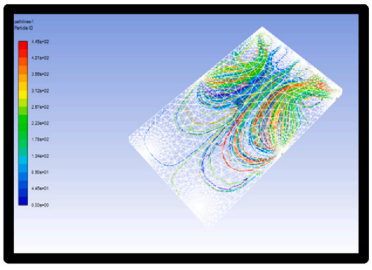	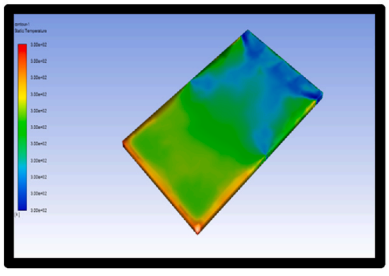

where.

T_{exp} = Experimentally measured temperature
T_{sim} = Temperature obtained from the simulation
T_{env} = Environmental temperature

6. Resulting in an $R^2 = 70$ % that is acceptable [50]

Finally, Table 13 shows the values of BIAS and RMSE obtained by analyzing all the temperature variation data.

7. Discussion

To determine the flow direction, greater emphasis was placed on correctly choosing the dimensions, mesh, and turbulence model to replicate the flow behavior with greater precision. This procedure is not influenced by the difference between steady and transient states, unlike the temperature analysis. During the study of the simulation in steady state, the turbulence model that replicated best the fluid behavior was k-ω, because of the wall effect, the pipe is small, and the fluid is influenced by the roughness, causing the Reynolds Number to be very low. On the other hand, it was observed that the temperature profile obtained was significantly different from that presented by thermography. Because of this, a transient state simulation was performed to determine if a better result could be obtained. In Tables 8 and in effect, a closer comparison was reached, although isoline graphs were used, because the zones of temperature variation can be better appreciated by relating them to those of the thermography. Observing this, it is recommended to use the simulation in the transient state to better understand the behavior of flow as a function of time and obtain top results for the study of heat exchange phenomena. Another aspect to consider is the simulation conditions for the transient state. By having the functions

Table 9
Streamlines Comparison.

	According to Simulation	Experimental [13]
B1	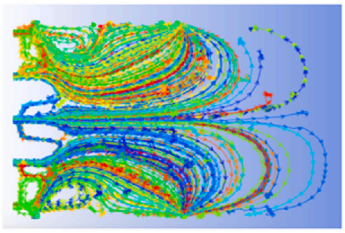	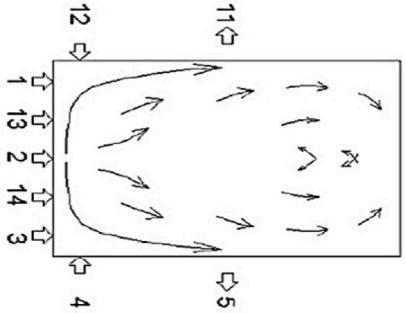
B4	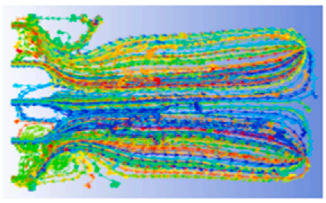	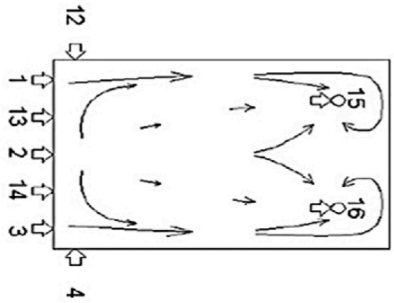

Table 10
Temperature Profile Comparison – Stationary.

	According to Simulation	Experimental [13]
B1	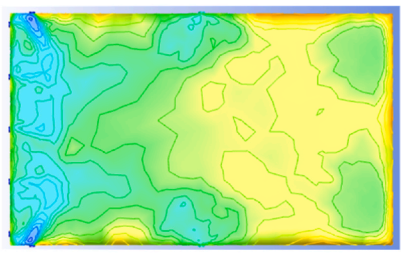	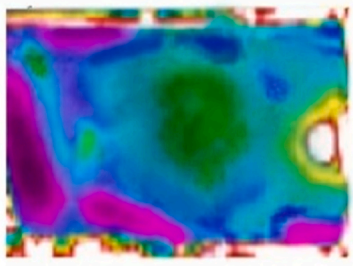
B4	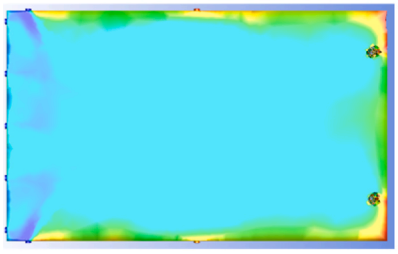	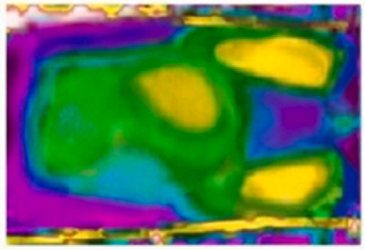

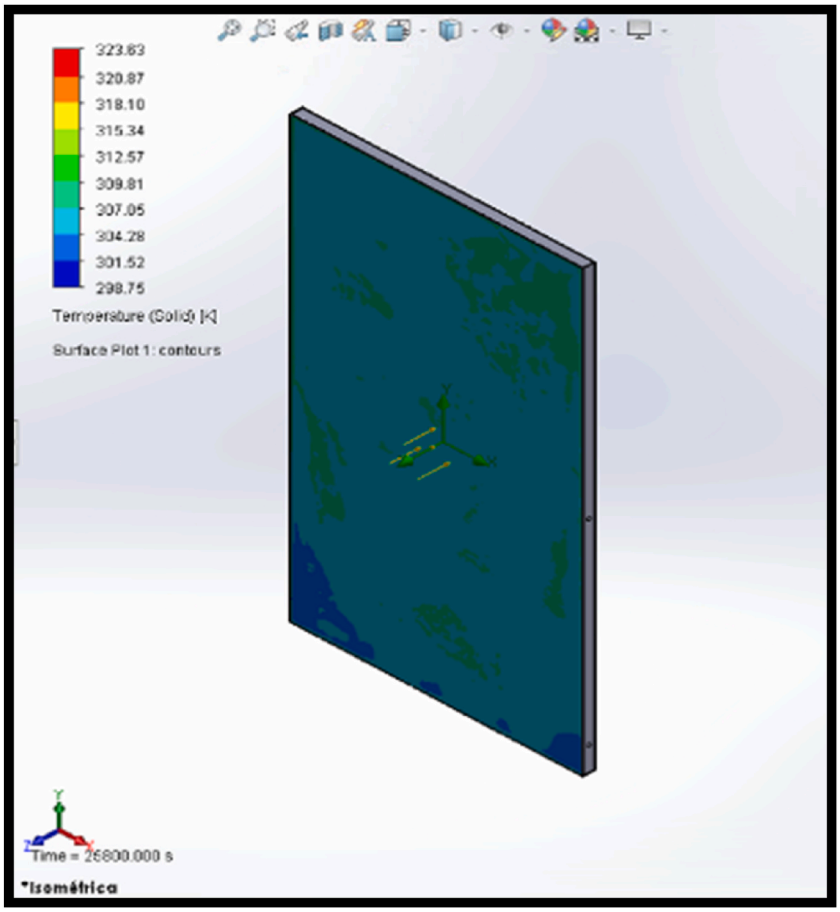

Fig. 12. Temperature contour for configuration B1.

concerning time for both the environmental temperature and the solar radiation, it was possible to perform a simulation with conditions as close as the real ones. It should be noted that the tables used to generate the function of temperature and radiation concerning time have different time steps for each day; for example, the day of August 12 has steps of 10 min for all the cases; on the 5th, almost the same; on the 17th, the pace is varied; and on the 16th, even more, which could affect the simulated results since in the graphs obtained with these data, peaks caused by aberrant data can be seen that appear abruptly. In this way, they obtained the values that were later used to determine the simulation error using the BIAS and RMSE formulas. For the latter, the variation was analyzed by comparing the simulated temperature with the one that was measured experimentally by Suzuki et al. [13]. Also, the environmental temperature, irradiation, and exit velocity were used to evaluate the correlation of these data with the difference between the temperatures. The values used to determine the correlation of the delta difference were obtained from four days of August 2019, these being days 5, 12, 17, and 26. In the case of configuration B1, I only had access to data from days 5, 12, and 26. Initially, these data had several aberrant values, so it was considered necessary to eliminate the day of August 12 to prevent these values from affecting the correlation result. Table 12 and Fig. 14 show the results. Then, to evaluate each piece of data concerning the temperature delta, it was concluded that the output speed and irradiance are independent of the delta values, while ambient temperature directly affects these values. Finally, BIAS and RMSE values were obtained, which show that there is a tendency to an error of approximately 1 or 2 °C for the simulated temperature obtained experimentally.

In this research, the economy of the PVT system was estimated. The PVT system costs 3.07 USD/W. The equivalent PVT system investment is 828.9 USD (if the average electrical power output is 270 W). The maintenance and operating cost considered is 10 % of the net present value (NPV). The benefit was calculated based on operation for 365 days a year. Table 14 lists the required economic parameters and assumptions for the economic analysis. The economic analysis and benefit results are tabulated in Table 15.

According to Table 15, the electricity production is 121.71 USD considering an annual irradiation of 6.5 kWh/m2 and a PV module of 270Wp. The NPV resultant is positive, and the IRR is higher than the benchmark yield. Moreover, the return of investment is less than 10 years.

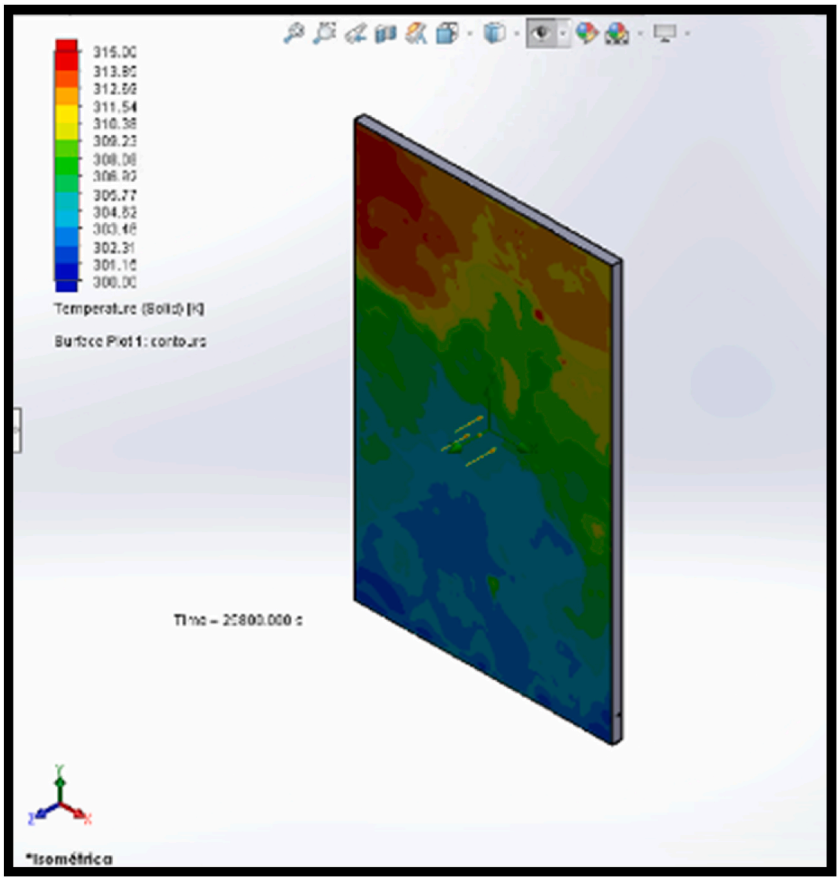

Fig. 13. Temperature contour for configuration B4.

8. Conclusion

The primary focus in determining flow direction was placed on selecting the appropriate dimensions, mesh, and turbulence model to precisely replicate flow behavior. Unlike temperature analysis, this procedure remained unaffected by the difference between steady and transient states. However, when studying the simulation in a steady state, a significant deviation was observed between the temperature profile obtained and that provided by thermography, for this different turbulence models were tested and analyzed to choose the one that better represent the behavior of the fluid resulting in the κ-ε model which help to determine the streamlines, but the deviation in temperature wasn't solved. To address this, a transient state simulation was conducted to seek improved results. While Table 8 facilitated a closer comparison, isoline graphs were employed, enhancing the visualization of temperature variations for better correlation with thermography data. Therefore, it is recommended to employ transient state simulations to gain a deeper understanding of flow behavior over time, yielding more accurate results for heat exchange studies. Additionally, it's crucial to consider the simulation conditions for the transient state, as they should closely mirror real-world conditions. The simulation included functions for environmental temperature and solar radiation over time. Notably, these functions had varying time steps for different days, potentially impacting simulated results due to abrupt peaks caused by aberrant data. The obtained values were subsequently used to assess the simulation error using BIAS and RMSE formulas. In this evaluation, the simulated temperature was compared with experimentally measured data from Suzuki et al. [13], along with environmental temperature, irradiation, and exit velocity, to determine the correlation with temperature differences. The data were collected from four days in August 2019: days 5, 12, 17, and 26. Configuration B1, however, had data only for days 5, 12, and 26, with the day August 12 omitted due to aberrant values. The results are presented in Table 12 and Fig. 14. In conclusion, the study found that output speed and irradiance are independent of temperature differences, while ambient temperature directly influences these values. The analysis of Bias and RMSE values indicates a consistent error of approximately 1–2 °C in the simulated temperature compared to the experimental measurements.

- The flow projections were accurate only for the B4 configuration. Streamlines projected for the B1 configuration did not match the simulation results.
- Heat Exchange: Stationary In steady state, the B1 configuration simulation more accurately replicated temperature profiles compared to the B4 simulation.

Table 11
Temperature Contour Comparison – Transient.

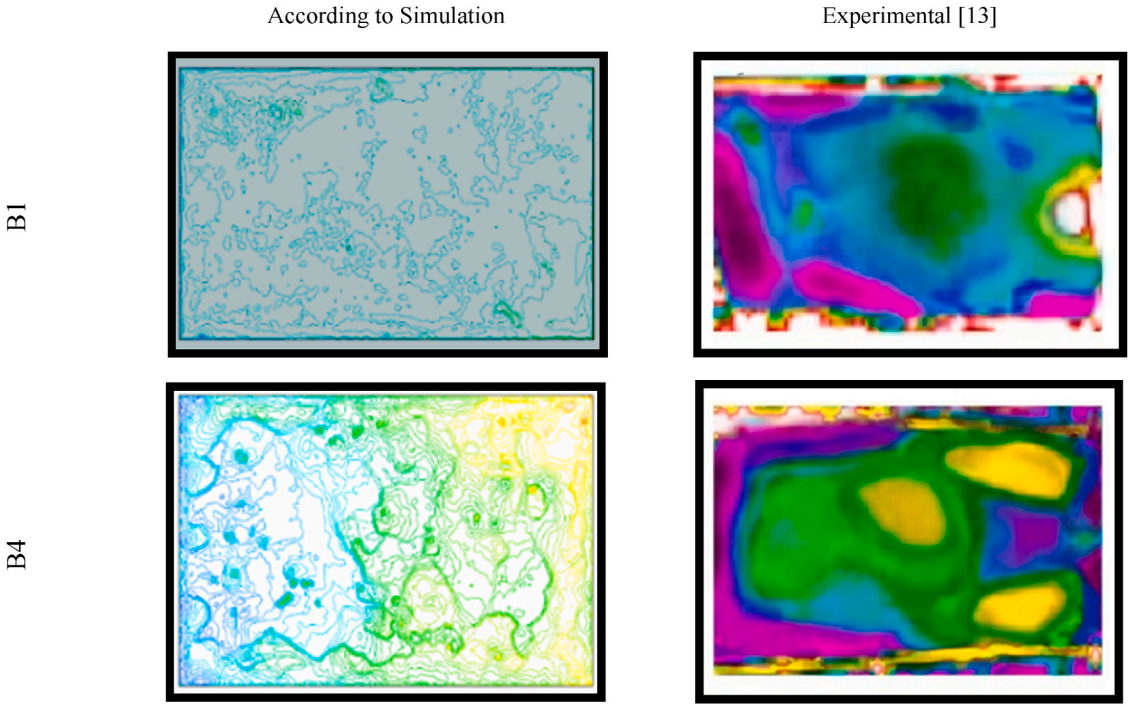

Table 12
Comparison data.

Solar Radiation [W/mˆ2]	Environmental Temperature [°C]	Simulation Temperature [°C]	Outlet Speed [m/s]	Delta [°C]
736.920	33.542	31.921	0.2425	0.0360
736.920	33.542	34.900	0.2184	−2.9430
889.829	37.181	28.948	0.1610	0.4460
889.829	37.181	28.951	0.1540	0.4430
922.092	38.060	34.330	0.9790	0.7600
922.092	38.060	35.280	0.9070	−0.1900
941.457	40.300	28.642	0.2170	2.9670
941.457	40.300	28.647	0.1730	2.9620
502.571	42.022	30.221	0.1653	2.2070
502.571	42.022	30.441	0.1601	1.9870

- Heat Exchange: Transient: When comparing temperature profiles, some color variations coincided, suggesting a successful simulation.
- Refrigeration: The B1 configuration is optimal for achieving uniform cooling in the photovoltaic panel.
- Validation: Output velocity and solar irradiation do not significantly affect the temperature difference (delta), while environmental temperature shows an acceptable correlation with an Rˆ2 value of 0.7.
- Bias and RMSE Analysis: The BIAS and RMSE values indicate a temperature error within an acceptable margin of approximately 2 °C. This error is influenced by the environmental temperature, becoming more pronounced as the experimental environment warms up.
- A positive NPV means that the present value of expected returns (cash inflows) is higher than the initial investment. It indicates that the investment is expected to generate more value than it costs, considering the time value of money and the discount rate used for the calculation.

Recommendations

Unlike the steady state, two series were used, one of temperature and the other of radiation, both about time, to refine the simulation results and thus obtain the graphs shown. Therefore, it is recommended to use this method to improve the accuracy of the

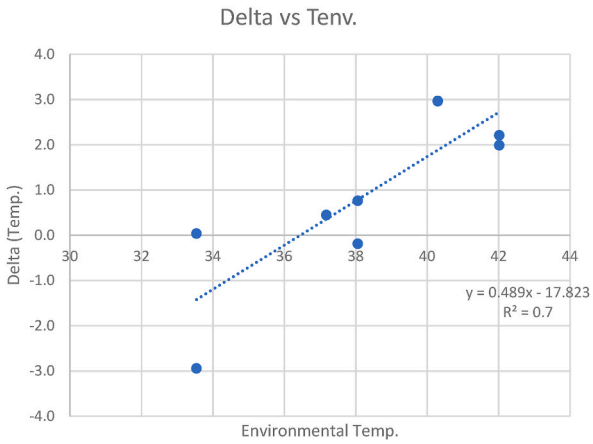

Fig. 14. Graph of the relationship between ambient temperature and temperature difference.

Table 13
BIAS & RMSE.

Simulation Temperature [°C]	Delta T [°C]
35.280	−0.1900
31.921	0.0360
28.642	2.9670
30.221	2.2070
28.948	0.4460
34.330	0.7600
34.900	−2.9430
28.647	2.9620
30.441	1.9870
28.951	0.4430
BIAS (T)	0.8675
RMSE (T)	1.8991

Table 14
Required economic parameters and assumptions.

Equipment investment (USD)	Maintenance and operating costs (USD/year)	Design life (year)	Electricity price (USD/kW·h)	Benchmark yield (%)	Depreciation rate (%)
828.9 USD	163.155	25	0.19	10	5

Table 15
Economic analysis and benefit results.

Annual Cash Flow due to Electricity Production (USD)	NPV	Internal Rate of Return (IRR) (%)	Recovery period of static investment (year)
121.71	388.2	14.15	6.81

simulation.

CRediT authorship contribution statement

Guido Abril-Macias: Writing – original draft, Writing – review & editing, Software, Methodology, Data curation. **J. Peralta:** Supervision. **E. Delgado:** Validation, Supervision. **I. Sosa:** Visualization, Validation, Supervision, Resources, Investigation, Conceptualization. **D. Avilés:** Visualization, Validation.

Declaration of competing interest

The authors declare that they have no known competing financial interests or personal relationships that could have appeared to influence the work reported in this paper.

References

[1] D. Henner, Full Report, 2017.
[2] O. Ellabban, H, B.F. Abu-Rub, Renewable energy resources: current status, future prospects and their enabling technology, Renew. Sustain. Energy Rev. 39 (2014) 748–764.
[3] H. Rezk, M. A, G.C. Abdelkareem, Performance evaluation and optimal desing of stand-alone solar PV-battery system for irrigation in isolated regions: a case study in Al Minya (Egypt), Sustain. Energy Technol. Assessments 36 (2019).
[4] M. Alobaid, Improving thermal and electrical efficiency in photovoltaic thermal systems for sustainable cooling system integration, Journal of Sustainable Development of Energy, Water and Environment Systems II (6) (2017) 305–322.
[5] E. Touti, M. Masmali, Fterich, H. Chouikhi, Experimental and numerical study of the PVT design impact on the electrical and thermal performances, Case Stud. Therm. Eng. 23 (2023).
[6] E. Radziemska, The effect of temperature on the power drop in crystalline silicon solar cells, Renew. Energy 28 (2003) 1–12.
[7] L. S. M., F.F. Piotrowski, Feasibility of water-cooled photovoltaic panels under the efficiency and durability aspects, Sol. Energy 207 (2020) 103–109.
[8] A.W. Kandeal, A.K. Thakur, M.R. Elkadeem, M.F. Elmorshedy, Z. Ullah, R. Sathyamurthy, S.W. Shanshir, Photovoltaics performance improvement using different cooling methodologies: a state-of-art review, J. Clean. Prod. 273 (2020).
[9] M. Mattei, G. Notton, C. Cristofari, M. Muselli, P. Poggi, Calculation of the polycrystalline PV module temperature using a simple method of energy balance, Renew. Energy IV (31) (2006) 553–567.
[10] N. Aste, C. Del Pero, F. Leonforte, M. Manfren, Performance monitoring and modeling of an uncovered photovoltaic-thermal (PVT) water collector, Sol. Energy 135 (2016) 551–568.
[11] M. Fuentes, M. Vivar, J. de la Casa, J. Aguilera, An experimental comparison between commercial hybrid PV-T and simple PV systems intended for BIPV, Renew. Sustain. Energy Rev. 93 (2018) 110–120.
[12] M P C M S, K S M, Performance of photovoltaic water pumping systems under the influence of panel cooling, Renewable Energy Focus 31 (2019) 31–44.
[13] M. Suzuki Valenzuela, Improving thermal distribution in water-cooled PV modules and its effect on RO permeate recovery, Water II (13) (2021) 229–260.
[14] K., K.P. Kim, Hot Spotting and Second Breakdown Effects on Reverse IV Characteristics for Mono-Crystalline Si Photovoltaics, IEEE Energy Conversion Congress and Exposition, 2013, pp. 1007–1014.
[15] K., K.P. Kim, "Photovoltaic Hot Spot Analysis for Cells with Various Reverse-Bias Characteristics through Electrical and Thermal simulation.," IEEE 14th Workshop on Control and Modeling for Power Electronics, 2013.
[16] A. B. K. T. D., S.S. Pandian, Fire hazards and overheating caused by shading faults on photo voltaic solar panel, Fire Technol. II (52) (2016) 349–364.
[17] H. L. P., H.M. Teo, An active cooling system for photovoltaic modules, Appl. Energy I (90) (2012) 309–315.
[18] H. B. A., G.P. Bahaidarah, Uniform cooling of photovoltaic panels: a review, Renew. Sustain. Energy Rev. 57 (2016) 1520–1544.
[19] G. Gan, Effect of air gap on the performance of building-integrated photovoltaics, Energy VII (34) (2009) 913–921.
[20] R., S.U. Stropnik, Increasing the efficiency of PV panel with the use of PCM, Renew. Energy 97 (2016) 671–679.
[21] S A A A A N Z A-H Y, J.H. Alsaqoor, The impact of phase change material on photovoltaic thermal (PVT) systems: a numerical stud, International Journal of Thermofluids 18 (2023).
[22] J. K. K., N.B. Siecker, A review of solar photovoltaic systems cooling technologies, Renew. Sustain. Energy Rev. 79 (2017) 192–203.
[23] S. P. F., L.S.A. Pennisi, Low-power cool bypass switch for hot spot prevention in photovoltaic panels, ETRI J. VI (33) (2011) 880–886.
[24] M. H. V. M. P., S.M. Dhimish, Novel hot spot mitigation technique to enhance photovoltaic solar panels output power performance, Sol. Energy Mater. Sol. Cell. 179 (2018) 72–79.
[25] M. Dhimish, V. Holmes, B. Mehrdadi, M. Dales, P. Mather, Output-power enhancement for hot spotted polycrystalline photovoltaic solar cells, IEEE Trans. Device Mater. Reliab. I (18) (2018) 37–45.
[26] K K H, A.F. Niazi, Hot-spot reduction and shade loss minimization in crystalline-silicon solar panels, J. Renew. Sustain. Energy III (10) (2018).
[27] C. S. K., H.H. Jubayer, CFD analysis of convective heat transfer from ground mounted solar panels, Sol. Energy 133 (2016) 556–566.
[28] A., A.M. Shahsavar, Energy and exergy analysis and optimization of a novel heating, cooling, and electricity generation system composed of PV/T-heat pipe system and thermal wheel, Renew. Energy 203 (2023) 394–406.
[29] O.R. Alomar, O.M. Ali, Energy and exergy analysis of hybrid photovoltaic thermal solar system under climatic condition of North Iraq, Case Stud. Therm. Eng. 28 (2021).
[30] O.R. Alomar, O.M. Ali, B.M. Ali, V.S. Qader, O.M. Ali, Energy, exergy, economical and environmental analysis of photovoltaic solar panel for fixed, single and dual axis tracking systems: an experimental and theoretical study, Case Stud. Therm. Eng. 51 (2023).
[31] O.A.B.S.O. Hamdoon, Performance analysis of hybrid photovoltaic thermal solar system in Iraq climate condition, Therm. Sci. Eng. Prog. 17 (2020).
[32] O.A.O.A.S. Ali, Energetic and exegetic performance analysis of flat plate solar collector under variables heat transfer coefficient and inlet water temperature, Case Stud. Therm. Eng. 28 (2021).
[33] K. Hamzat, A Z S I O, L M A, Advances in PV and PVT cooling technologies: a review, Sustain. Energy Technol. Assessments 47 (2021).
[34] M. Jurčević N. S., M.-K. I., C. D., A. M., G. E., P. A., Investigation of heat convection for photovoltaic panel towards efficient design of novel hybrid cooling approach with incorporated organic phase change material, Sustain. Energy Technol. Assessments 47 (2021).
[35] G.S. Menon, M. S., E. J., A. D. D. S., A. P. V., M. P. S., Experimental investigations on unglazed photovoltaic-thermal (PVT) system using water and nanofluid cooling medium, Renew. Energy 188 (2022) 986–996.
[36] J. S. M. J. H., K.Y. Lee, Development of solar radiation spectrum-controlled emulsion filter for a photovoltaic-thermal (PVT) system, Energy Convers. Manag. 287 (2023).
[37] A., Z.O. Almuwailhi, Investigating the Cooling of Solar Photovoltaic Modules under the Conditions of Riyadh, Journal of King Saud University–Engineering Sciences, 2021.
[38] A. R. Z. M., R.S. Hadipour, An efficient pulsed-spray water cooling system for photovoltaic panels: experimental study and cost analysis, Renew. Energy 164 (2021) 867–875.
[39] Z. Özcan, L. Bilir, G M, S E, C N Y, Cooling channel effect on photovoltaic panel energy generation, Sol. Energy 230 (2021) 943–953.
[40] S., E.M. Nazari, Impact of frame perforations on passive cooling of photovoltaic modules: CFD analysis of various patterns, Energy Convers. Manag. 239 (2021).
[41] U., Y.J. Rajput, Comparison of heat sink and water type PV/T collector for polycrystalline photovoltaic panel cooling, Renew. Energy 116 (2018) 479–491.
[42] J. Badules, M. Vidal, A. Boné, J. Llop, R. Salcedo, E. Gil, F.J. García-Ramos, Comparative study of CFD models of the air flow produced by an air-assisted sprayer adapted to the crop geometry, Comput. Electron. Agric. 149 (2018) 166–174.
[43] M. G. D. G. H, C.F. Chowdhury, Experimentally validated CFD simulations predicting wind effects on photovoltaic modules mounted on inclined surfaces, Sustain. Energy Technol. Assessments 30 (2018) 201–208.
[44] J. Danielewicz, B. Sniechowska, M.A. Sayegh, N. Fidorow, H. Jouhara, Three-dimensional numerical model of heat losses from district heating network pre-insulated pipes buried in the ground, Energy 108 (2016) 172–184.
[45] S. Harikrishnan S. Tiwari, Effect of skewness on flow and heat transfer characteristics of a wavy channel, Int. J. Heat Mass Tran. 120 (2018) 956–969.
[46] S. Misha Abdulalah A. L., Tamaldin N., Mohd Rosli M. A., Sachit F. A., Simulation CFD and experimental investigation of PVT water system under natural Malaysian weather conditions, Energy Rep. 6 (2020) 28–44.
[47] Hernández R. Morales Amador Núñez M. A., Fernández Lorenzo I., Elena Parnás V. B., Validación del modelo en CFD de una nave ante cargas de viento con análisis estacionario, Ing. Hidraul. Ambient. XLIII (4) (2022) 27–37.

[48] M. Rodríguez, Trabajo Fin de Máster Máster Universitario en Ingeniería Industrial Análisis de modelos de un captador solar plano en régimen transitorio, 2016. Sevilla.
[49] X. Zhang, A.U. Weerasuriya, K.T. Tse, CFD simulation of natural ventilation of a generic building in various incident wind directions: comparison of turbulence modelling, evaluation methods, and ventilation mechanisms, Energy Build 229 (2020).
[50] C.H. Feng Makino Y., Yoshimura M., Rodríguez-Pulido F. J., Estimation of adenosine triphosphate content in ready-to-eat sausages with different storage days, using hyperspectral imaging coupled with R statistics, Food Chem. 264 (2018) 419–426.